UNCLASSIFIED

SECURITY CLASSIFICATION OF THIS PAGE

2

ATION PAGE DTIC FILE COPY

1a REPORT SECURI UNCLASSI

AD-A225 996

1b RESTRICTIVE MARKINGS

2a SECURITY CLASS

3 DISTRIBUTION/AVAILABILITY OF REPORT

APPROVED FOR PUBLIC RELEASE
DISTRIBUTION IS UNLIMITED

2b DECLASSIFICATION/DOWNGRADING SCHEDULE

4 PERFORMING ORGANIZATION REPORT NUMBER(S)

5 MONITORING ORGANIZATION REPORT NUMBER(S)

AFOSR-TR- 90 0875

6a NAME OF PERFORMING ORGANIZATION
Princeton University

6b OFFICE SYMBOL (If applicable)

7a NAME OF MONITORING ORGANIZATION
AFOSR/NA

6c ADDRESS (City, State and ZIP Code)
Princeton, NJ 08544

7b ADDRESS (City, State and ZIP Code)
BUILDING 410
BOLLING AFB, DC 20332-6448

8a NAME OF FUNDING/SPONSORING ORGANIZATION AFOSR/NA

8b OFFICE SYMBOL (If applicable)
AFOSR/NA

9 PROCUREMENT INSTRUMENT IDENTIFICATION NUMBER
AFOSR
89-0091

8c ADDRESS (City, State and ZIP Code)
BUILDING 410
BOLLING AFB, DC 20332-6448

10 SOURCE OF FUNDING NOS

PROGRAM ELEMENT NO	PROJECT NO.	TASK NO.	WORK UNIT NO.
61102F	2307	A2	

11. TITLE (Include Security Classification)
(U) Investigation of Supersonic Boundary Layer Transition and Turbulent Structure

12. PERSONAL AUTHOR(S)
A. J. Smits and R. B. Miles

13a TYPE OF REPORT	13b TIME COVERED	14 DATE OF REPORT (Yr., Mo., Day)	15. PAGE COUNT
Final Technical	FROM 12/1/88 TO 3/1/90	1990/7/24	19

16. SUPPLEMENTARY NOTATION

17 COSATI CODES			18 SUBJECT TERMS (Continue on reverse if necessary and identify by block number)
FIELD	GROUP	SUB GR	Supersonic Turbulent Boundary Layer, Rayleigh Scattering, Non-Intrusive Instrumentation
	20,04		

19. ABSTRACT (Continue on reverse if necessary and identify by block number)

Abstract

This report is the final report for AFOSR Grant 89-0091, awarded under the Defense University Research Instrumentation Program (Control No. 08450-0810). In it, we describe the research progress made possible with the equipment purchased under this grant, and the manpower supplied by Princeton University as part of cost sharing.

1990

20. DISTRIBUTION/AVAILABILITY OF ABSTRACT

UNCLASSIFIED/UNLIMITED ☒ SAME AS RPT ☐ DTIC USERS ☐

21 ABSTRACT SECURITY CLASSIFICATION
UNCLASSIFIED

22a NAME OF RESPONSIBLE INDIVIDUAL	22b TELEPHONE NUMBER (Include Area Code)	22c OFFICE SYMBOL
Len Sakell	202-767-4935	AFOSR/NA

DD FORM 1473, 83 APR EDITION OF 1 JAN 73 IS OBSOLETE

UNCLASSIFIED

SECURITY CLASSIFICATION OF THIS PAGE

FINAL TECHNICAL REPORT

Defense University Research Instrumentation Program
Control No. 08450-0810

Investigation of Supersonic Boundary Layer Transition and Turbulent Structure

by

A.J. Smits and R. B. Miles

July 15, 1990

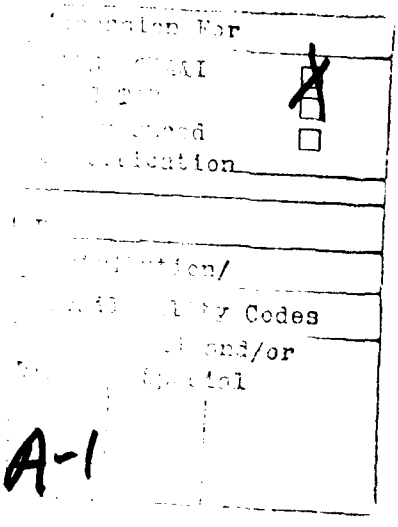

Att. Dr. L. Sakell
Dr. J. M. McMichael

Abstract

This report is the final report for AFOSR Grant 89-0091, awarded under the Defense University Research Instrumentation Program (Control No. 08450-0810). In it, we describe the research progress made possible with the equipment purchased under this grant, and the manpower supplied by Princeton University as part of cost sharing.

1. Introduction

The Gasdynamics Laboratory at Princeton University is conducting a major program of research to study the structure of supersonic turbulent boundary layers, with support under AFOSR Grants 89-0420, 90-0217, and 90-0261 . The principal aim of this research is to describe the structure of the instantaneous large-scale motions in supersonic turbulent boundary layers, especially in complex flows where pressure gradients, shock waves, streamline curvature, and separation are present. The results will contribute towards the development of predictive turbulent models for complex flows, and suggest strategies for the control of supersonic turbulent boundary layers.

Past progress in the study of high Reynolds number compressible flows has been hampered by the difficulty of obtaining sufficient information on the space and time distribution of the fluctuating density and velocity field. LDV systems and hot-wire anemometers only provide single-point information, and time-histories of fluctuating quantities, which permit the study of instantaneous structure, have only recently become available (Spina and Smits, 1987). To overcome some of these difficulties, the Laser and Applied Physics Laboratory with support under AFOSR Grant 86-0191 has developed new non-intrusive techniques for the simultaneous measurement of instantaneous velocity profiles and density cross-sections in high speed air flows. These methods significantly expand our capability for experimental measurements in turbulent supersonic flows.

The instrumentation obtained under this grant have helped to apply these new tools to flows of fundamental fluid mechanical interest in the 8" x 8" Mach 3 facility at the Gas Dynamics Laboratory. In particular, we have used the Rayleigh scattering to visualize the instantaneous density field in a wide variety of flows: zero pressure gradient, high Reynolds number turbulent boundary layers, a shock wave/boundary layer interaction generated by a 16^{o} compression corner, a fully-developed free shear layer formed by the separation of a boundary layer of a backward-facing step, the reattachment of this shear layer on a 20^{o} ramp, and two different three-dimensional interactions: one generated by a blunt fin with a circular leading edge, and another by a sharp fin at a 20^{o} angle of attack.

In addition, we have reconfigured the RELIEF technique in an entirely new way to make it a much more robust technique, capable of being used with a minimum of support, in terms of equipment and personnel. The RELIEF technique is a non-intrusive method to generate a time-gated image of moving oxygen

molecules. Time lines are written and tracked in air much as the hydrogen bubble technique writes and tracks time lines in water. In the early work, this method required the use of two lasers, overlapped in time and space, to write the line in air, and a third UV laser to interrogate the line a known time later. In our recent work, made possible by the purchase of a Nd:YAG laser with the support of the current grant, the two tagging lasers have been replaced with a much simpler and much more robust system consisting of a single laser (the YAG laser referred to above) and a Raman cell. This system eliminates the difficult and time-consuming alignment process which characterized the earlier system, and it is much less susceptible to vibration and rough handling. The interrogation system presently still requires an additional UV laser, but development of a suitable flashlamp source is progressing, and we anticipate that the flashlamp will replace the UV laser, perhaps by the end of this calender year.

Currently, we have obtained a wide variety of Rayleigh images, as suggested above, and some of these results are summarized below. The application of the RELIEF method to flows generated in the 8" x 8" MAch 3 facility is in progress, and we anticipate obtaining preliminary results by the end of this summer.

2. Progress Report on Results Obtained by the Rayleigh Scattering Technique

In this section, examples of these images are given, with a short explanation of their significance.

The images were made possible by using a high-power, Nd:YAG laser operating in the far-ultraviolet in conjunction with a high-sensitivity, far-ultraviolet camera. By focusing the laser into a thin sheet of light and passing it through the wind tunnel, cross-sectional images of the air density can be recorded by direct Rayleigh scattering. For the pictures shown here, the illumination is with a Quantel International YG661 laser operating in the vicinity of .266 microns with a pulse duration of 4 nsec, so the cross-sectional image is frozen in time. The 8" x 8" Mach 2.9 tunnel was fitted with UV transmitting quartz windows so that the laser sheet could be passed through the flow field. The high-sensitivity camera observed the scattering at 90^{o} and images could be recorded up to the laser pulsing rate of 10 Hz.

The presence of water in the air can have a strong effect on the interpretation of these images, even for extremely low water concentrations (parts per million). Upstream of the nozzle, where it is in the form of water vapor, its

Rayleigh cross section is small. However, as the flow expands through the nozzle, the water molecules can agglomerate into very small ice clusters of the order of 30 nanometers in diameter (Wegener and Stein 1968). When they are present in sufficient numbers, these small particles dominate the Rayleigh signal. Quantitatively, therefore, the images obtained in air give the density of these ice clusters rather than the density of air. Now, it appears that the ice crystal density is nearly proportional to the local air density, except in regions where the temperature rises to the point where the ice returns to the vapor phase. There are two main consequences: we lose some resolution near the wall, where the frictional heating increases the temperature, and strong shocks become visible as lines separating bright zones (low temperature) from dark zones (high temperature).

In some cases, nitrogen was used as the working fluid. The nitrogen gas was flashed from liquid nitrogen, and therefore its water content was negligibly small. Here, the images indicate the true instantaneous local density. However, since the Rayleigh scattering cross-section of nitrogen molecules is very much smaller than that corresponding to the ice clusters found in air, it was very much more difficult to obtain a high level of contrast. It was particularly difficult to reduce the background scattered light to acceptable levels, and the images taken in nitrogen do not show the boundary layer details very well. In contrast, the shock structure is shown very clearly, and the local brightness of the image gives the shock strength directly.

Unless otherwise stated, the Reynolds number based on the incoming boundary layer momentum thickness was either 30,000 or 80,000. The scale of each image, from top to bottom, is about two boundary layer thicknesses, regardless of the Reynolds number. The resolution is on the order of several hundred micrometers, which corresponds to about 1 or 2% of the boundary layer thickness, depending on the Reynolds number. The flow is always from right to left, and the images show the incoming boundary layer on the right. Further details of the upstream flow conditions are given in Table 1.

a. Fundamental Studies of Turbulent Boundary Layers in Supersonic Flows

These experiments are designed to elucidate physical models and mechanisms that are particular to compressible turbulence, such as the effects of compressibility on the nature of the large-scale motions, the scaling laws for high Reynolds number supersonic turbulent flows, direct compressibility effects that cause the exchange of turbulence energy among the vorticity, entropy and sound modes, and the transport of heat and momentum by compressible turbulent motions.

Some images of Rayleigh scattering in a zero pressure gradient, high Reynolds number boundary layer in air are shown in Figure 1. In a qualitative fashion, these images show that there are well-defined individual structures present in the incoming boundary layer. The dark areas of the image represent low density regions characteristic of high temperatures, and the bright areas are typical of the high densities found in the free stream. This result is expected appears to hold even when the Rayleigh signal is produced by scattering from ice clusters. Intermittent penetration of freestream fluid deep into the boundary layer is clearly visible.

Current work is directed towards the quantitative interpretation of these images, which means in effect determining the connection between the local image intensity which is related to the local density of the ice clusters, and the density of the air at that point. The preliminary results are encouraging, in that the intensity of the measured Rayleigh signal in the outer part of the boundary layer appears to be nearly proportional to the local air density. If this proportionality is confirmed, we can proceed to examine the statistics of the density field. Space correlations will be particularly useful, since they indicate the spatial distribution of the "average" large scale motions. They are also relatively insensitive to the calibration of the Rayleigh signal, and should provide useful information even when the density of ice crystals is changing because of temperature effects. We will also be able to extend the fractal analysis performed by Prof. Sreenivasan to study the influence of Mach number on the fractal dimension of the turbulent/non-turbulent interface, a study which has important implications for mixing.

In additional experiments, we intend to obtain double-pulsed images to study the evolution of the larger scales in time. In previous work, Smith and Smits (1988) obtained high speed schlieren movies of a Mach 3 boundary layer to show

the convection of large-scale motions inclined at about 45°. However, the schlieren method is sensitive to the density gradient, and it integrates across the optical path. Details of the motions are completely obscured. In contrast, double-pulsed Rayleigh images will show the evolution of the density (directly) in a plane, and they can be compared directly with similar images obtained by numerical simulations and flow visualizations at lower Mach and Reynolds numbers. We believe that these time-evolving images are crucial for the development of dynamically accurate models. This work has the technical support of the Applied Physics Laboratory headed by Prof. Miles.

Furthermore, we intend to make a quantitative evaluation of the validity of the Strong Reynolds Analogy, by studying simultaneously the turbulent density and velocity fields in a flat plate Mach 2.9 turbulent boundary layer using both hot-wire anemometry and Rayleigh scattering/RELIEF techniques.

b. Shock Wave Boundary Layer Interactions Generated by Compression Corners

Experiments have been performed in 16° and 24° compression corner interactions with two purposes: (1) to clarify the dynamic nature of the interaction between the large-scale motions and the shock movement, and (2) to determine the connection between the velocity, density fields, and their connection with the instantaneous wall pressure and heat transfer. Preliminary images taken in a streamwise plane in an air flow for the 16° case are shown in Figure 2.

The large scale motions observed in the incoming boundary layer can interact strongly with the shock wave, as shown in some of the figures. It appears from these images, and previous work by Dolling (1990), that the unsteady shock motion is closely coupled with the strength and frequency content of the incoming boundary layer structure. As far as we know, these images are the first to reveal the instantaneous shock structure, and the first to show the direct influence of the turbulence on the unsteady shock motion. At this stage, the particular characteristics of the turbulence that result in the strong coupling is not known, although we suspect that only large motions, with a high degree of coherence can interact directly with the shock. Further data analysis may lead to deeper insights. For example, image processing techniques can be used to generate space correlations of the fluctuating density field, and reveal the dynamic connection between the incoming motions, the shock motion, and the

turbulence distortion. Since the space correlation is relatively insensitive to the calibration of the Rayleigh signal, these measurements will be valid even in regions where the density of ice clusters is affected by temperature effects.

When the plane of the light sheet is oriented parallel to the freestream direction, the image gives an instantaneous plan view of the large scale organization of the boundary layer. When the plane of light is tilted so that it makes an angle of about 20^{o} with the plane of the ramp, a most remarkable wrinkling of the reattachment shock is made visible, particularly for the 24^{o} case (Figure 3). This visualization of the instantaneous wrinkling of the shock sheet is the first ever obtained.

In future work, we intend to couple the Rayleigh flow visualizations with the wall-pressure measurements, so that we can determine directly the coupling between the incoming turbulent motions and the wall pressure. We hope to use the Rayleigh scattering images to obtain quantitative data on the density field, such as rms intensity levels, probability density distributions, and space correlations. Using these quantitative techniques, we may be able to establish the statistical properties of the average large-scale motion interacting with the shock wave.

c. Swept Shock Wave Boundary Layer Interactions Generated by Sharp Fins

The swept interaction generated by sharp fin at an angle of attack is one of the simplest three-dimensional shock wave boundary layer interactions, and it has been studied for a wide range of boundary and initial conditions. Recent survey papers by Settles and Dolling (1986, 1990) summarize the present state of our understanding in a very comprehensive way. What is clear from these papers is that very little is known regarding the instantaneous flow field, including the shock unsteadiness and the distortion of the turbulence.

To begin an exploration of these issues, some Rayleigh scattering images were obtained in an interaction generated by a sharp fin at a 20^{o} angle of attack in an air flow (see Figure 4). The field of view is in a plane normal to the wall (that is, normal to the floor of the tunnel), and parallel to the incoming freestream direction. The upstream boundary layer can be seen on the right of these pictures, as are the separation shock (the line coming forward from the triple point at about 45^{o}), and the freestream shock (seen as the vertical line emerging from the triple point). A shock going downstream (possibly the

reattachment shock) can also be seen coming from the triple point. The most notable features are probably the strong distortion of the separation shock, which is far from straight and seems to be strongly influenced by the incoming turbulence, the rapid thickening of the flow downstream of this shock (remember this is a three-dimensional flow, and the flow to the left of the separation shock is coming out of the picture at angles up to 45^{0}), the up and down movement of the triple point, and the highly contorted turbulent motions downstream of the interaction. These images are the first ever images of a three-dimensional supersonic flow which are not spatially averaged, as in shadowgraph or schlieren.

Future work will extend the Rayleigh scattering work to incorporate spanwise views, together with simultaneous measurements of the wall pressure fluctuations, in an attempt to determine more precisely the link between the incoming turbulence and the shock unsteadiness.

d. Three-Dimensional Shock Wave Boundary Layer Interactions Generated by Blunt Fins

Another three-dimensional interaction of great interest is the interaction induced by a blunt fin or circular cylinder mounted normal to the surface on which the incoming boundary layer develops. This work is sponsored by NASA-Lewis, Program Manager Warren Hingst. This geometry:

(i) generates a large scale, unsteady three-dimensional, vortical separated flowfield whose length scales in all three dimensions are controlled largely by the fin leading edge diameter, D. Hence, generating flowfields of various physical scales is greatly simplified.

(ii) the length scale of the unsteady separation shock wave can be similarly controlled by changing D. Doubling D will double the shock motion length scale, apparently independently of the boundary layer thickness. This suggests that there is little connection between the scale of the shock motion and the scale of the incoming turbulence.

(iii) the spectral content of the wall pressure fluctuations generated by the unsteady shock wave can be changed predictably simply by changing D. With a fixed incoming boundary layer, an increase in D decreases the mean shock frequency and vice-versa.

The Rayleigh scattering images shown in Figure 5 were obtained in a vertical plane on the centerline of the interaction, parallel to the incoming freestream

direction. The working fluid for these images was air. The overall image is rather similar to that seen in the sharp fin case discussed above, see Figure 4). The incoming boundary layer can be seen on the right of these pictures, as are the separation shock (the line coming forward from the triple point at about 45^{o}), and the freestream shock (seen as the vertical line emerging from the triple point). A shock going downstream can also be seen emanating from the triple point.

This flow was also investigated using dry nitrogen instead of air, thereby avoiding the scattering from ice clusters. In the case of nitrogen, it was found that the Rayleigh signal was considerably weaker, as might be expected, and it was difficult to achieve sufficient contrast to make boundary layer visible. However, strong discontinuities such as shocks could be distinguished clearly (see Figure 6). The flow inside the separated zone, where Figure 5 just shows a black region, is now plainly visible. The shock structure near the foot of the blunt fin is shown to be highly unsteady, and it seems to be made up of a number of cells, which may indicate the presence of a number of horse-shoe vortices, as had been suggested by Korkegi (1976) from mean wall pressure measurements.

The other notable features are the strong distortion of the separation shock (which is again far from straight and seems to be strongly influenced by the incoming turbulence), and the up and down movement of the triple point.

As in the sharp fin study, future work will extend the Rayleigh scattering work to incorporate spanwise views, together with simultaneous measurements of the wall pressure fluctuations, in an attempt to determine more precisely the link between the incoming turbulence and the shock unsteadiness.

3. Laser System Development

The original specification for the Quantel Model YG661 laser system was 300 mJ per pulse in the green (532.0 nm) and 35 mJ per pulse in the ultraviolet (266.0 nm). We purchased the system without the ultraviolet option and developed our own ultraviolet doubling options to achieve a maximum of 100 mJ per pulse at 266.0 nm. For the Rayleigh scattering work reported here, the images were taken with 30 to 50 mJ per pulse.

The timing electronics are a critical feature for capturing two-dimensional images. The YG661 laser requires a complex timing circuit in order to be synchronized to an external source. To accomplish this, we have built an

electronic signal converter which locks the laser pulse to the camera sweep rate in order to generate synchronized two-dimensional images. A Stanford Research Systems timing box is then used to Q-switch the laser and simultaneously gate the camera. Camera gate widths as low as 1 sec are used so that background from the room lights is virtually eliminated. This makes the data acquisition possible with the room lights on and eliminates significant background noise including laser flashlamp scattering.

The YG661 laser is particularly useful as a source for the tagging step in the RELIEF flow tagging work. The high energy (300 mJ) and short pulse length (5 nsec) at 532.0 nm, means that the gain in our stimulated Raman shifter is very high. As a consequence, we get excellent conversion from 532.0 nm to 580.0 nm, and we can use those two frequencies, focused simultaneously into the test section, for flow tagging. Preliminary experiments on flow tagging are currently underway at the Gas Dynamics Laboratory using this laser system.

References

Hayakawa, K., Smits, A.J. and Bogdonoff, S.M. (1984) AIAA Journal, 22:889-895.

Korkegi, R.H. (1976) AIAA Journal, 14:597-600

Miles, R., Cohen, C., Connors, J., Howard, P., Huang, S., Markovitz, E. and Russell, G. (1987) Optics Letters, 12:861.

Settles, G.S. and Dolling, D.S. (1976) In AIAA Progress in Astronautics and Aeronautics: Tactical Missile Aerodynamics, Ed. M. Hemsch and J. Nielsen, 104:297-379, AIAA, New York.

Settles, G.S. and Dolling, D.S. (1990) AIAA Paper 90-0375.

Shen, Z. H., Smith, D.R. and Smits, A.J. (1990) AIAA Paper 90-.

Smith, M.W. and Smits, A.J. (1988) AIAA Paper 88-0500.

Smith, M.W., Smits, A.J. and Miles, R.B. (1989) Optics Letters, 14:916-918.

Spina, E.F. and Smits, A.J. (1987) J. Fluid Mech., 182:85-109.

Wegener, P.P. and Stein, G.D. (1968) 12th Intern. Symp. on Combustion, 1183-1191.

	CASE 1	CASE 2
p_o (Nt/m^2)	6.8×10^5	6.8×10^5
T_o (^oK)	265 ± 5	265 ± 5
M_e	2.84 ± 0.04	2.84 ± 0.04
U_e (m/s)	575 ± 20	575 ± 20
$(\rho U)_e$ (kg/m^2s)	500 ± 30	500 ± 30
Re_e/m	$6.5 \pm 0.5 \times 10^7$	$6.5 \pm 0.5 \times 10^7$
(mm)	26 ± 1.5	12 ± 1.0
C_f	$.001 \pm .0001$	$.0011 \pm .0001$

Table 1. Incoming flow conditions.

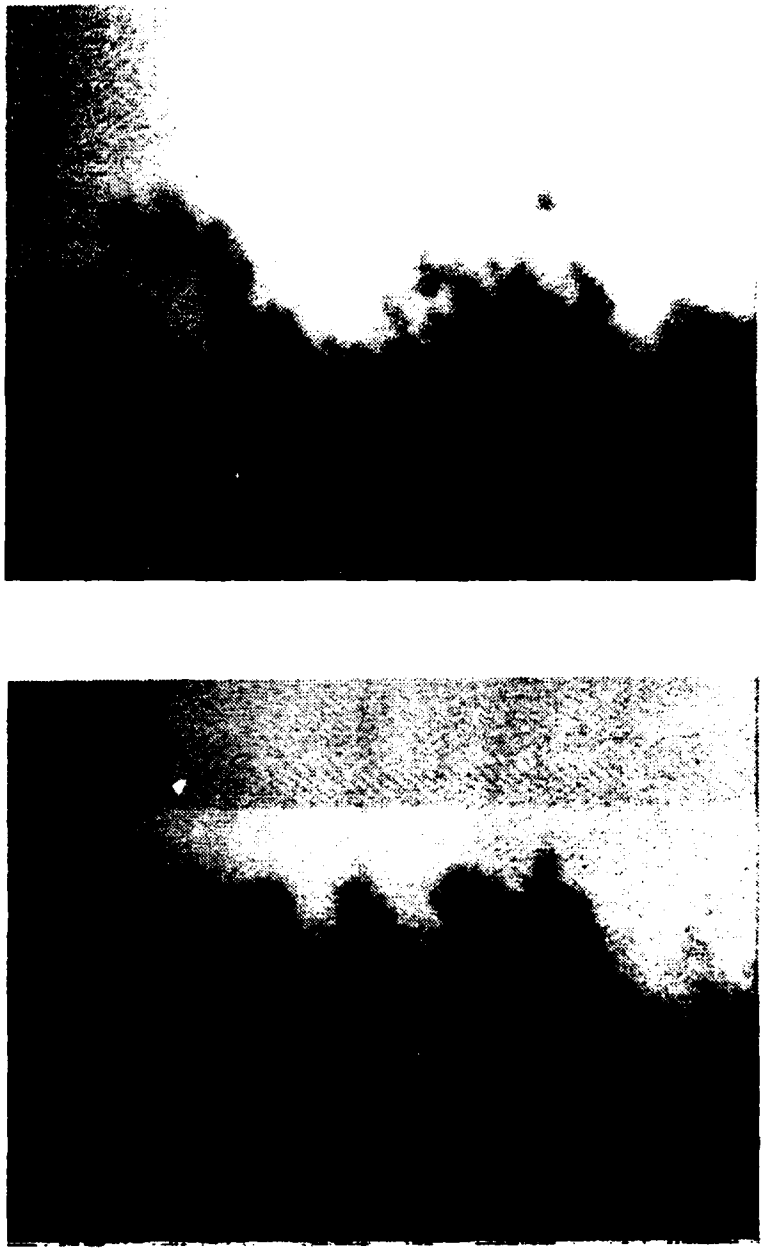

Figure 1a. Streamwise images of Mach 2.9 boundary layer flow in air (Case 1). See Table 1 for details. Flow is from right to left.

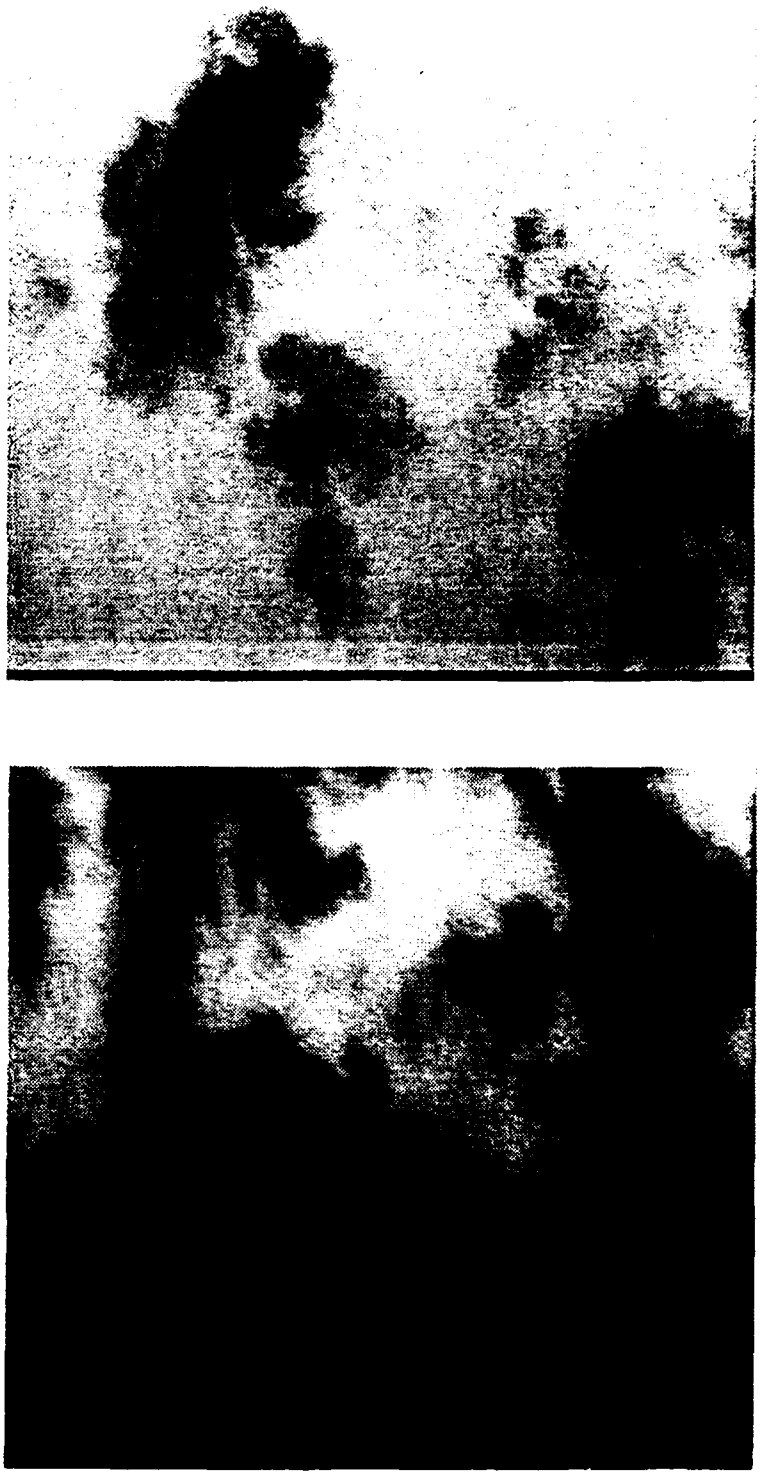

Figure 1b. Planview images of Mach 2.9 boundary layer flow in air (Case 1). See Table 1 for details. Flow is from top to bottom of the picture. The wall distance as a fraction of the boundary layer thickness 0.91 and 0.54.

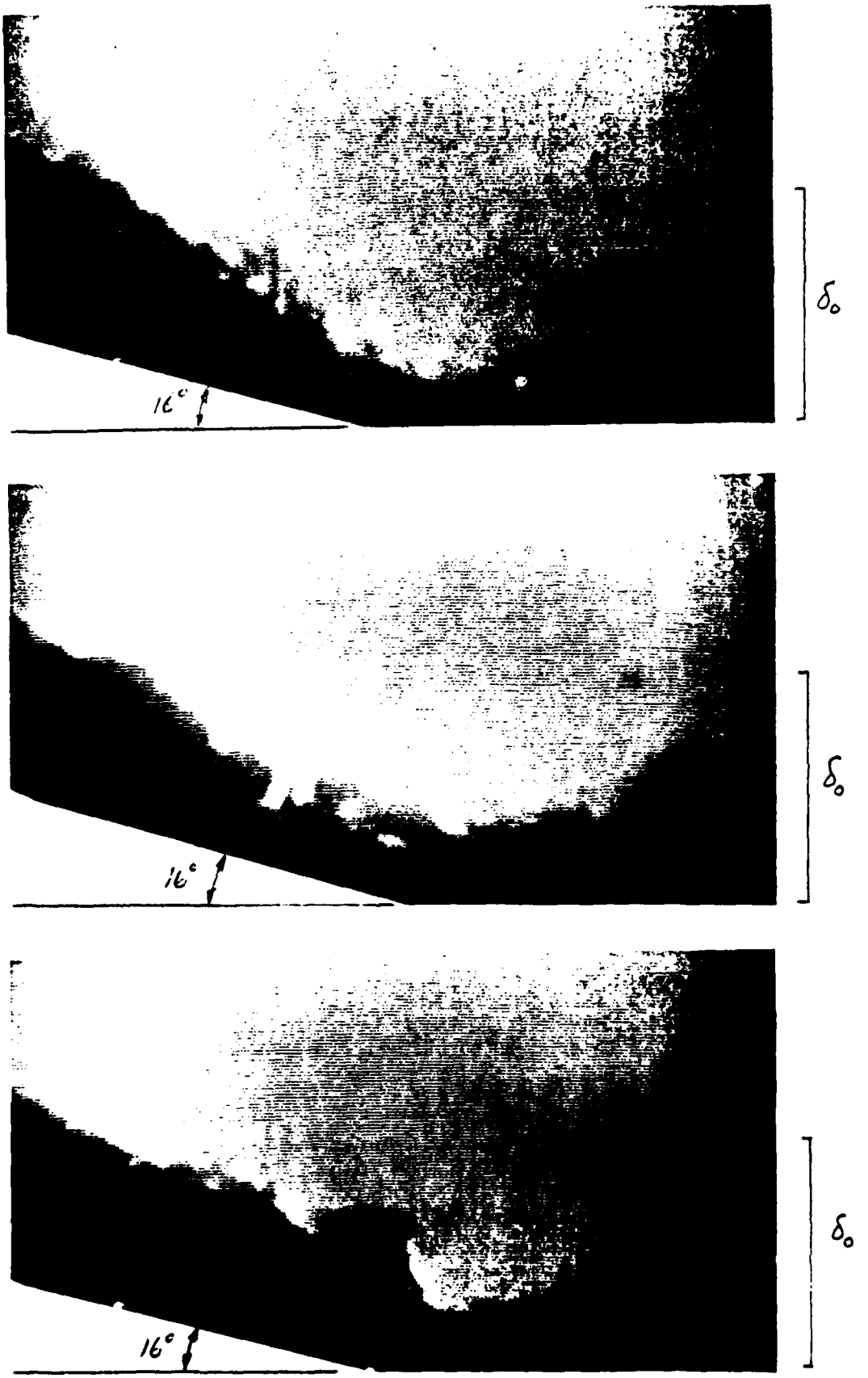

Figure 2. Streamwise images of shock wave boundary layer interaction generated by a 16° compression corner in an air flow. See Table 1 for details of the incoming boundary layer (Case 1). Flow is from right to left.

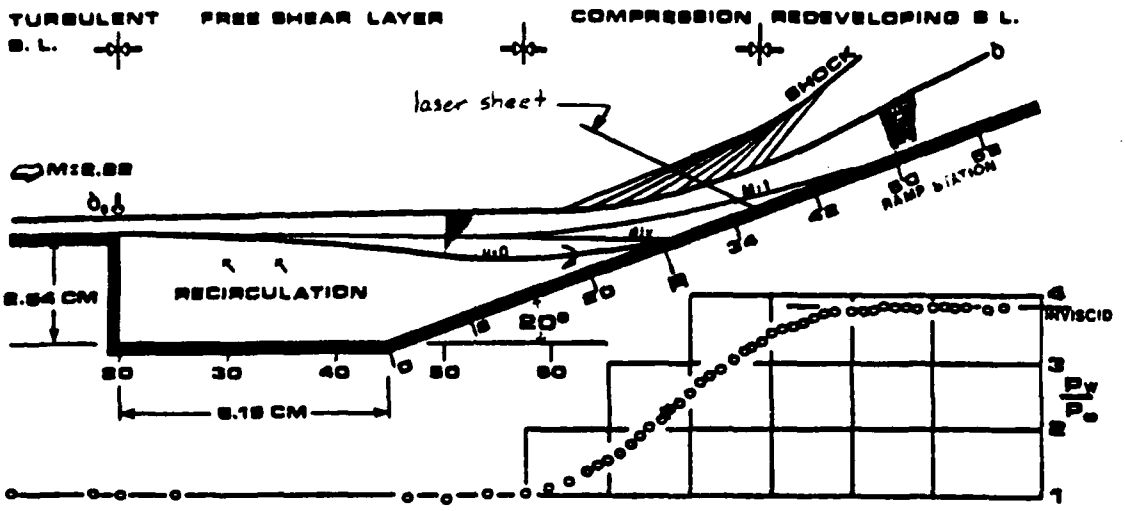

Figure 3a. Geometry for the formation of a free shear layer and its subsequent attachment on a 20^{0} ramp.

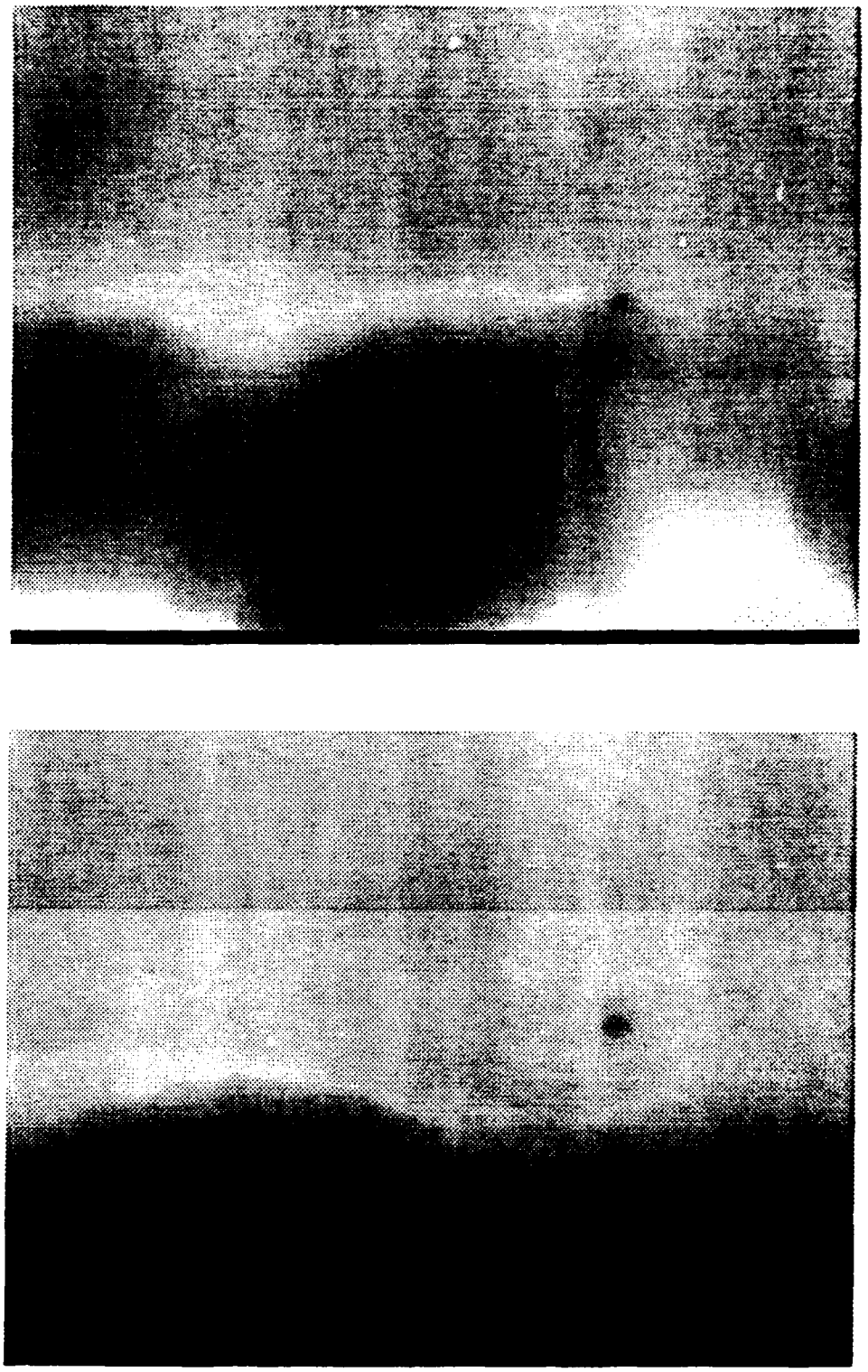

Figure 3b. Images of the attachment region of a freeshear layer on a 20^{o} ramp in an air flow. The laser sheet orientation is as shown in Fig. 3a. Flow is from top to bottom of the picture. Shocks show up as regions where the brightness increases (this is true as long as the temperature rise is relatively small). These images indicate that the shock is strongly wrinkled by the incoming turbulence.

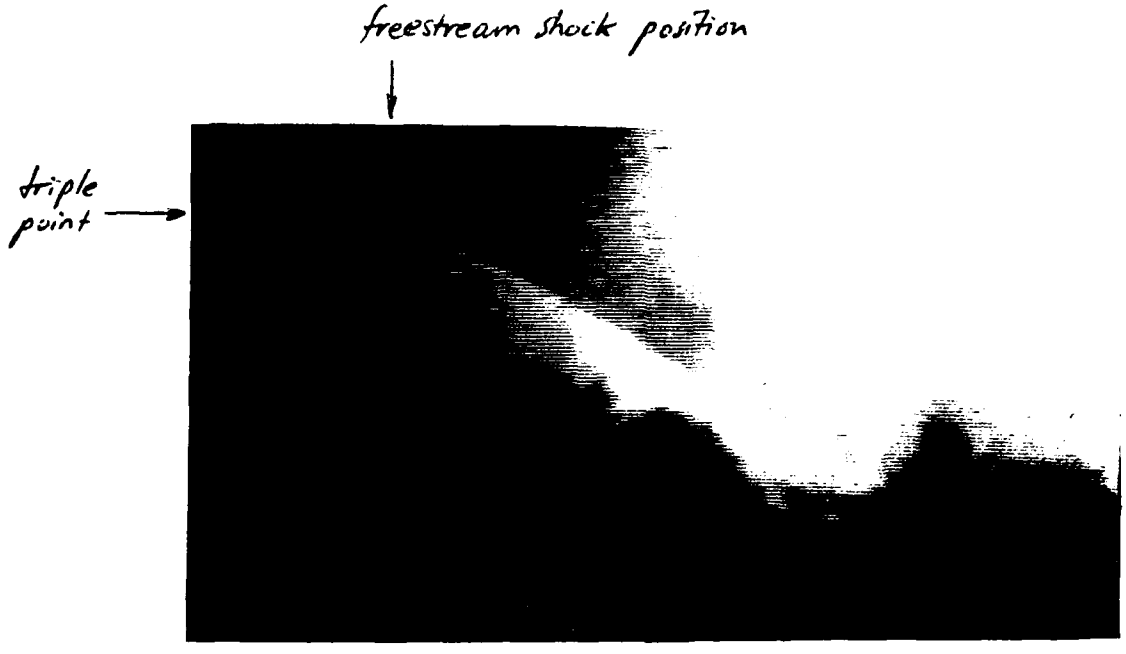

Figure 4. Image of the three-dimensional interaction generated by a sharp fin at a 20^{o} angle of attack in an air flow. The incoming flow is from right to left (Case 2 in Table 1), and behind the first shock the flow is out of the plane of the image at angles varying from 20 to 45^{o}.

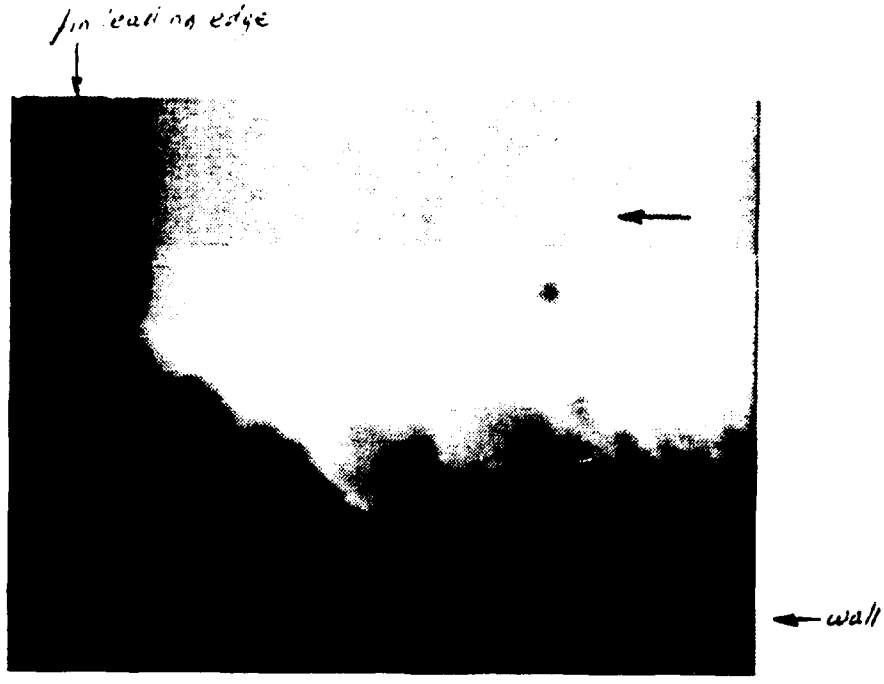

Figure 5. Image of the three-dimensional interaction generated by a blunt fin in an air flow. The plane of the laser sheet coincides with the centerline of the interaction. The incoming flow is from right to left (Case 1 in Table 1).

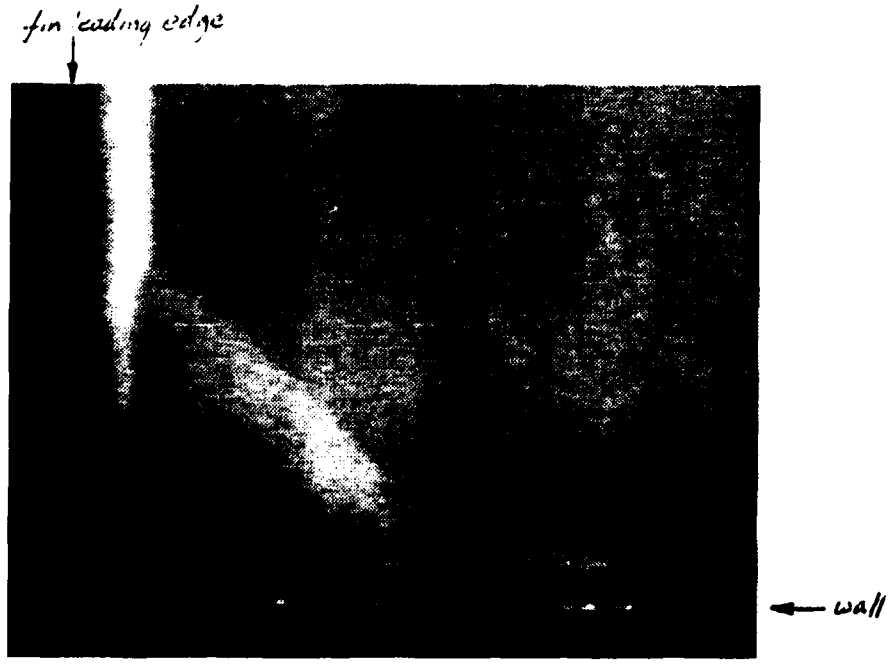

Figure 6. Image of the same three-dimensional interaction shown in Figure 5, this time in a nitrogen flow. As in Figure 5, the plane of the laser sheet coincides with the centerline of the interaction. The incoming flow is from right to left (Case 1 in Table 1).